Prog Addit Manuf (2017) 2:179–191
https://doi.org/10.1007/s40964-017-0028-9

FULL RESEARCH ARTICLE

Nanoparticle improved metal materials for additive manufacturing

Jan T. Sehrt[1] · Stefan Kleszczynski[1] · Christian Notthoff[2]

Received: 11 May 2016 / Accepted: 28 July 2017 / Published online: 30 August 2017

Abstract A variety of laser systems and powder materials is available for additive manufacturing processes such as powder bed fusion of metallic parts (laser beam melting). The required energy density for a sufficient melting of powder materials strongly depends on the optical properties of the used powder (e.g., absorption, reflection and transmittance). During laser irradiation a moving melt pool is generated in the laser heat affected zone. Re-solidification of the molten particles results in interconnected welding lines similar to those of traditional welding processes. Here, the layer by layer approach combined with a selective laser exposure in cross-sectional areas of the parts enable the generation of 3D structures from the powder bed. The mechanical properties of such fabricated structures are usually comparable to the mechanical properties of the bulk material the powder particles are made of. In this paper, a proof of principle is demonstrated to receive improved mechanical or other properties of parts being manufactured by laser beam melting. The approach addresses laser beam melting of the commonly available powder materials tool steel (1.2709) and Hastelloy X (2.4665) which are additionally modified with nanoparticles (Al_2O_3) on their surfaces. Due to the shortage of these two available nanoparticle modified materials (about 100 g each) only relatively small test specimens are manufactured and, therefore, only limited typical characteristic values could be determined. However, the nanoparticle modified and laser beam molten 3D structures were systematically characterized by optical and scanning electron microscopy, energy-dispersive X-ray microanalysis, micro hardness indentation and etching analysis. It turns out that modification of the educt powder surfaces with nanoparticles prior to laser beam melting can improve e.g., mechanical properties of the generated 3D structures.

Keywords Additive manufacturing · Powder bed fusion (laser beam melting) · Laser-generation of nanomaterials · Tool steel (1.2709) and Hastelloy X (2.4665)

1 Introduction

Additive manufacturing (AM) technologies allow the production of solid 3D parts with high complexity by joining formless materials in a layer by layer approach. Rapid developments in the field of AM, especially for powder bed fusion processes, led to a new point of view from prototype production to Rapid Manufacturing applications. Following this trend our research activities are illustrated in this paper which in turn meet tomorrow's requirements. Laser beam melting (LBM) is a neutral term which is defined and described in the VDI-Guideline 3405 [1]. It belongs to the category of powder bed fusion processes according to the standard ISO/ASTM 52900 [2]. Furthermore, it is defined as "additive manufacturing process…in which thermal energy selectively fuses regions of a powder bed" [2]. Among the large number of AM processes based on the same working principle and materials, laser beam melting (LBM) is also known as trademark names such as direct metal laser sintering (DMLS, EOS GmbH), selective laser

✉ Jan T. Sehrt
jan.sehrt@uni-due.de

[1] University of Duisburg-Essen, Institute for Product Engineering, Manufacturing Technology, Lotharstr. 1, 47057 Duisburg, Germany

[2] University of Duisburg-Essen, Institute for Combustion and Gasdynamics, Nanoparticle Process Technology and Center for Nanointegration Duisburg-Essen (CENIDE), Lotharstr. 1, 47057 Duisburg, Germany

melting (SLM, SLM Solutions Group AG), LaserCUSING (Concept Laser GmbH), laser metal fusion (LMF, Trumpf Laser- und Systemtechnik GmbH) or direct metal printing (DMP, 3D Systems, Inc.). Using this technology 3D solid parts are made layer by layer from fine metal powder which is locally molten by a focused laser beam and connected to the underlying solid layer. The manifold possibilities for manufacturing unique structures by laser AM techniques are responsible for pushing different methods, such as LBM or laser sintering, into the focus of research.

Previous research activities have shown that conventional metal alloys processed by LBM provide a high degree of density and acceptable mechanical properties [3–5], which are similar to those of traditionally manufactured parts of the same material. However, the process specific high temperature gradients produced by the local melting of a very small region and the rapid solidification may cause high residual stresses, which can—dependent on the material properties and process parameters—induce part deformations, cracks or voids [6]. On the other hand, the rapid solidification process could be useful for the creation of novel microstructural features. Schmidtke et al. showed that using LBM for processing of an Al–Sc alloy the precipitation of the intermetallic Al_3Sc phase can be suppressed [7]. After additional heat treatment, it was possible to adjust a defined amount of nano-crystalline precipitations, which improved the materials fracture toughness significantly. Gu et al. demonstrated that novel alloy systems can be created for the LBM process by mixing pure Cu powder with different amounts of CuSn and CuP powders [8]. Different microstructural manifestations were observed, featuring different appearances of components dissolubility and agglomeration that depend on the mixing ratio and applied process parameters. Similar observations were made by Gu et al. for a mixture of W, Ni and graphite powder processed by LBM to create in situ $WC/Ni_2W_4(M_6C)$ cemented carbide based hardmetals [9].

Integration of nanoparticles during AM processes is another current field of interest. Yugang et al. [10] and Chiu et al. [11] improved the mechanical and thermal properties of parts manufactured by vat photopolymerization processes using nano modified photosensitive resins.

Also LBM is in the focus of research with the aim to enhance different material properties. Gu et al. processed nanocomposite parts using different kinds of regular LBM materials and different kinds of small sized reinforcement materials [12–16]. They also investigated TiC/Ti nanocomposite parts [12–14]. The in situ creation of TiC particle reinforced Ti–Al matrix composites by LBM was also reported by Gu et al. [17]. In this approach, mechanical alloying was used to produce powder mixtures of elemental Ti, Al and graphite powders with nano-crystalline microstructures inside of the powder particles. After processing via LBM these materials showed a slight increase of the nano-scaled crystal grains. However, the finally generated microstructure was still refined and provided sub micrometer reinforcing structures. Gu et al. also studied the influence of processing parameters of the LBM machine on densification activity, microstructure, nanohardness and wear behavior of LBM-processed parts [12]. Their TiC/Ti nanocomposite powder system was milled and contained 15 wt% TiC with an average particle size of 50 nm and 85 wt% Ti-particles with a mean particle diameter of 22.5 µm. It turned out that too little (90 J/mm^3) and too high (360 J/mm^3) volumetric laser energy densities lead to poor material characteristics. Appropriate material characteristics could be obtained using volumetric energy densities of 120–180 J/mm^3. Using the same composite material of TiC/Ti Gu et al. also investigated the influence of the TiC content on the material characteristics [14]. As a result, the optimal TiC content was determined to be around 12.5 wt%. In Gu et al. [13] compared ball-milled TiC/Ti nanocomposite powder versus directly mechanical mixed nano-TiC/Ti powder using LBM. They found that the densification level of ball-milled TiC/Ti nanocomposite powder was generally larger compared to solely mechanical mixed nano-TiC/Ti powder. Almost fully dense (>98%) TiC/Ti parts could be produced. The TiC-reinforced phases in the LBM nanocomposite material had a lamellar nanostructure with thickness on the nanoscale. Additionally, Gu et al. performed similar investigations on the material characteristics with other material combinations such as TiC particle reinforced AlSi10 Mg nanocomposite material parts [15, 16]. Chang et al. studied the influence of different SiC powders with a polyangular structure and different particle sizes with a mean particle size D_{50} of 50, 15 and 5 µm on the microstructure and mechanical properties of the LBM-processed composite parts at a weight ratio AlSi10 Mg to SiC of 80:20 [18]. They found that best material characteristics can be obtained using the smallest particle size of $D_{50} = 5$ µm.

Other works could show that the integration of nanoparticles has a positive influence on continuous wave laser structuring [19] or pulsed laser structuring [20, 21]. These studies focused on laser structuring processes.

This article investigates LBM of different nanoparticle modified metal-materials such as a nickel base alloy Hastelloy X (2.4665) and tool steel (1.2709). These powders commonly used for LBM are mixed and combined with Al_2O_3-nanoparticles. Such a material combination has not been in the focus of research yet. Here, we report on the influence of nanoparticles on properties such as micro hardness or local material composition obtained in the final structures after LBM. The expected advantages of this approach to alternative material systems using LBM are e.g., a significant increase of mechanical properties, heat

resistance and wear resistance. This might lead to new application fields and new developments in future.

2 Experimental methods and technologies

For the experiments commercially available standard powder materials were used and modified accordingly. This surface modification of the base metallic materials, tool steel (1.2709) and Hastelloy X (2.4665) was carried out prior to the LBM process. The impact on micro hardness and the resulting microstructure are also investigated. The experimental methods are divided into nanoparticle modification of the standard materials, processing of the new composite materials by LBM and the microstructural and mechanical properties characterization.

2.1 Nanoparticle modification of standard materials (powder preparation)

Both standard materials, tool steel (1.2709) and nickel base alloy Hastelloy X (2.4665), are commercially available and have. Tool steel is known for its excellent mechanical properties especially after age hardening. Thereby the tensile strength increases from 1100 ± 100 MPa (as built) to 2050 ± 100 MPa (after age hardening) according to the material data sheet EOS MaragingSteel MS1. The nickel based alloy Hastelloy X is heat and corrosion resistant and has a high tensile strength up to 850 ± 40 MPa (as built/XY-direction) and good elongation at break values of 29 ± 8% (as built/XY-direction) according to the material data sheet EOS NickelAlloy HX. The material composition of parts being manufactured with both standard materials can be seen in Table 1.

Modification of these two materials was carried out by adsorption of 1 wt% aluminum oxide nanoparticles on the metal powder surfaces. Therefore, commercially available aluminum oxide nanoparticles (sigma aldrich) were dispersed in ethanol (1 wt%) and pretreated by ultra-sonication for 5 min to achieve a homogeneous particle size distribution. To further improve colloidal dispersion properties, the suspension was exposed to laser irradiation. Briefly, optimized pulsed laser fragmentation conditions known to cause particle size reduction [22] were applied for 10 irradiation cycles in a free liquid jet using a picosecond laser system at 532 nm with 7.5 W and 100 kHz repetition rate. Subsequently 100 g of the metal powders were added to the nanoparticle suspension and the ethanol was removed resulting in 1 wt% surface adsorbed aluminum oxide nanoparticles onto the metal micrometer particles (see Fig. 1). Note that in this case ethanol was used to avoid unwanted corrosion of the metal powder. Additionally, exposure time of the metal particles was kept below 10 h to avoid unwanted reaction with the liquid environment.

Table 1 Material composition of the used standard materials according to EOS material data sheets

Hastelloy X (2.4665)		Tool steel (1.2709)	
Ni	Balance (wt%)	Fe	Balance (wt%)
Cr	20.5–23.0	Ni	17–19
Fe	17.0–20.0	Co	8.5–9.5
Mo	8.0–10.0	Mo	4.5–5.2
W	0.2–1.0	Ti	0.6–0.8
Co	0.5–2.5	Al	0.05–0.15
C	≤0.1	Cr	≤0.5
Si	≤1.0	Cu	≤0.5
Mn	≤1.0	C	≤0.03
S	≤0.03	Mn	≤0.1
P	≤0.04	Si	≤0.1
B	≤0.01	P	≤0.01
Se	≤0.005	S	≤0.01
Cu	≤0.5		
Al	≤0.5		
Ti	≤0.15		

2.2 LBM processing of the nanoparticle modified powder materials

For processing of nanoparticle modified materials an EOSINT M 270 machine from EOS GmbH was used. In contrast to the typical powder handling system in this machine, which spreads a new layer of powder automatically across the build platform unidirectionally, here a new layer of powder can only be applied manually. This time-consuming procedure is due to the small amount of modified standard materials (about 100 g per material), which is too insufficient for filling the powder reservoir of the machine. Nevertheless, the composite powder material was spread across a small build platform bidirectional by moving the powder heap from right to left followed by laser exposure, lowering the build platform, moving the recoating mechanism behind the powder heap, highering the build platform again up to one layer thickness below the previous layer and then moving the powder heap back from left to right to spread the following layer (cf. Fig. 2a).

Four cylindrical test specimens with a diameter of 7 mm and a height of around 2.3 mm were manufactured from each of the two composite materials, using a layer thickness of 40 µm during LBM. The test specimens are also directly fabricated onto the build platform without any support structures underneath (cf. Fig. 2b). Both new composite materials were processed according to the standard laser parameters of the standard powders,

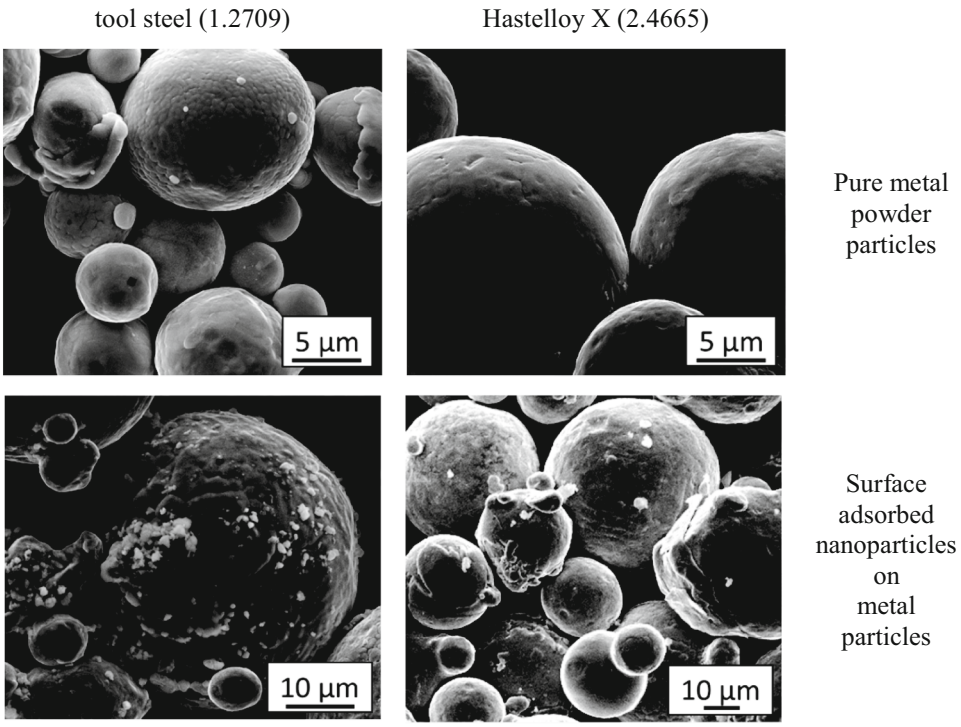

Fig. 1 SEM images of tool steel and Hastelloy X without and with surface adsorbed aluminum oxide nanoparticles

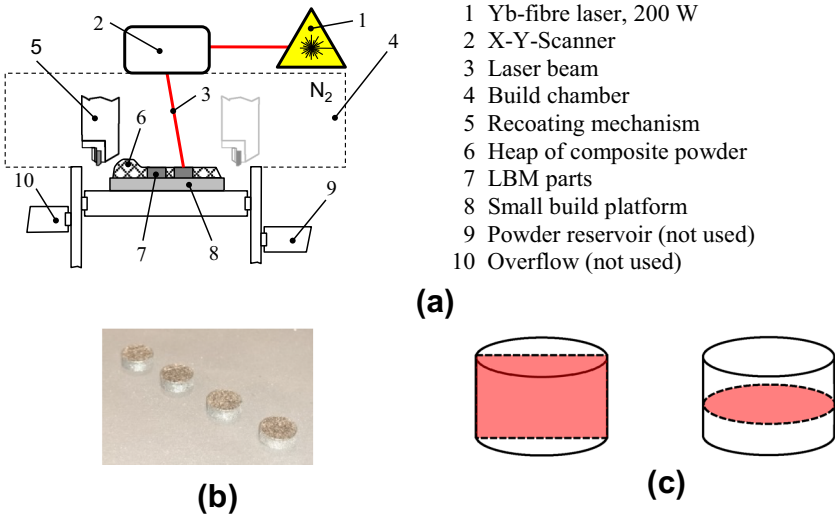

Fig. 2 Manual processing of nanoparticle modified materials **a** scheme of the LBM processing set-up, **b** test specimens fabricated by LBM, **c** illustration of two sectioning types: longitudinal (*left*) and transverse (*right*) for further analysis

knowingly, that these parameters are probably not ideal for production. The following table summarizes the most important process parameters being used for this investigations (Table 2).

2.3 Microstructural and mechanical properties characterization

A JEOL-JSM7500F cold field emission scanning electron microscope (SEM) is used for high resolution imaging of the Al_2O_3 precipitates. The acceleration voltage is typically 15 kV and a probe current of 60 pA was used for imaging. A Bruker Quantax 200 system equipped with a 30 mm^2 SSD crystal is attached to the SEM for energy dispersive X-ray spectroscopic (EDX) measurements. Quantification of the chemical composition is performed by the software ESPRIT (co. Bruker).

The produced specimens were cut lengthwise in buildup z-direction to allow microstructural inspection of the specimens' cross sections in x–z and x–y plane (cf. Fig. 2c). Each specimen was mounted in conductive embedding media and grinded to a smooth surface finish with silicon carbide paper increasing the grid size from 80 to 1200 in five steps. Subsequently the specimens were

Table 2 LBM process parameters applied for the composite materials

Standard material	Tool steel (1.2709)	Hastelloy X (2.4665)
Nanoparticle material	Al_2O_3	Al_2O_3
Laser power	195 W	138 W
Wave length laser	1060–1100 nm	1060–1100 nm
Hatch distance	0.1 mm	0.1 mm
Layer thickness	40 µm	40 µm
Scan speed	750 mm/s	600 mm/s
Volume energy density	65 J/mm^3	57.5 J/mm^3
Laser beam diameter	74 µm	74 µm
Laser peak intensity	11.33 kW/mm^2	8.02 kW/mm^2
Scan strategy	Rotated	Rotated
Inert gas atmosphere	Nitrogen	Nitrogen

polished to a mirror finish in two steps with 5 and 1 µm diamond solution. Optical microscopy (OM) was carried out with an Olympus BX 41 microscope. Micro hardness indentation was performed by a Zwick Z 3212 small load Vickers hardness tester. After porosity and EDX analysis the specimens were exposed to etching media for visualizing the microstructure. For the tool steel specimens V2A-etching solution, composed of 100 ml HCl, 100 ml H_2O, 10 ml HNO_3 and 0.3 ml pickling inhibitor, was used. The Hastelloy X specimens were exposed to an etching solution consisting of 50 ml distilled water, 150 ml HCl, 25 g Chrom(VI).

3 Results and discussion

3.1 Influence of nanomodification on the melting behavior

It could be observed that both composite powders could not be spread as smooth as the unmodified standard materials across the build platform due to a decreased flowability probably caused by the nanoparticles. Thus, small furrows could be detected on the powder surface which could influence the melting behavior. These furrows might be a result of increased Van der Waals forces between the powder particles due to the nanomodification of the surface. Figure 3 depicts microscope images showing the melting behavior of the two Al_2O_3 nanoparticle modified materials in comparison to the unmodified standard materials. It is obvious that the presence of nanoparticles clearly affects the melting behavior of the powder materials.

Figure 3a shows a very smooth and nearly perfect LBM-surface. Here the unique welding lines are consistently interconnected and fused together homogeneously in both directions laterally and front-end. In contrast to this the processed nanoparticle modified material Hastelloy X (2.4665) shows a different result. Here the LBM-surface appears rough and the welding lines seem to be fused together less homogeneously. The typical welding structure of the moving melt pool on the surface cannot be detected anymore compared to Fig. 3a. Also the welding lines of the nanoparticle modified material Hastelloy X are partly tipped with small dark crater like structures. In addition, a small elevation at the stripe overlap structure can be seen.

The standard tool steel 1.2709 shown in Fig. 3c shows a smooth and very good LBM-surface with just a limited amount of weld spatters on the surface. The interconnections of the welding lines are sufficient and good. The nanoparticle modified material tool steel (1.2709) in Fig. 3d shows a rough surface with small dark crater like structures. In addition, the welding lines vary in width laterally. These results clearly show that the used process parameters for manufacturing the nanoparticle modified materials are not ideal. Due to the characteristics of the welding lines of the nanoparticle modified materials it can be concluded that the laser energy density applied during melting is insufficient. This might indicate that the incorporated nanoparticles increase the required energy demand for a homogeneous melting process. Presumably, the temperature in the generated melt pool is not high enough to cause sufficient material flow and to wet adjacent material areas. Melt pool evolution is strongly dependent on a complex interaction of different physical processes, as laser beam absorption, evaporation, wetting of powder particles, heat conduction, capillary effects, surface tension, melt viscosity and melt pool dynamics [23–25]. For this reason, one possible explanation is that the Al_2O_3 nanoparticles influence the wetting behavior and/or affect the melt convection current, so that no ideal welding line can be formed. This is also the reason for the variation in width of the individual welding lines. The appearance is comparable with the qualification of new materials for the LBM process. To achieve good parameters for processing new materials the parameters need to be varied in a specific range. At too low energy densities during laser exposure inhomogeneities or even entire welding line interruptions can occur [2, 26, 27]. An increase of the energy density by adjusting mainly the laser parameters would probably lead to a more uniform welding structure in our case. Thus, we believe that the imperfect welding structure in case of nanoparticle modified powder materials is related to inappropriate LBM energy densities. But it can be seen clearly that the presence of nanoparticles influences the fusion process. Generally, the melting behavior of the modified materials could also adversely affect the process stability at LBM, e.g., by process breakdowns caused by collisions between the powder supply mechanism and the poor quality of the parts surfaces or the superelevated contours of the part. But the quality of the LBM processed

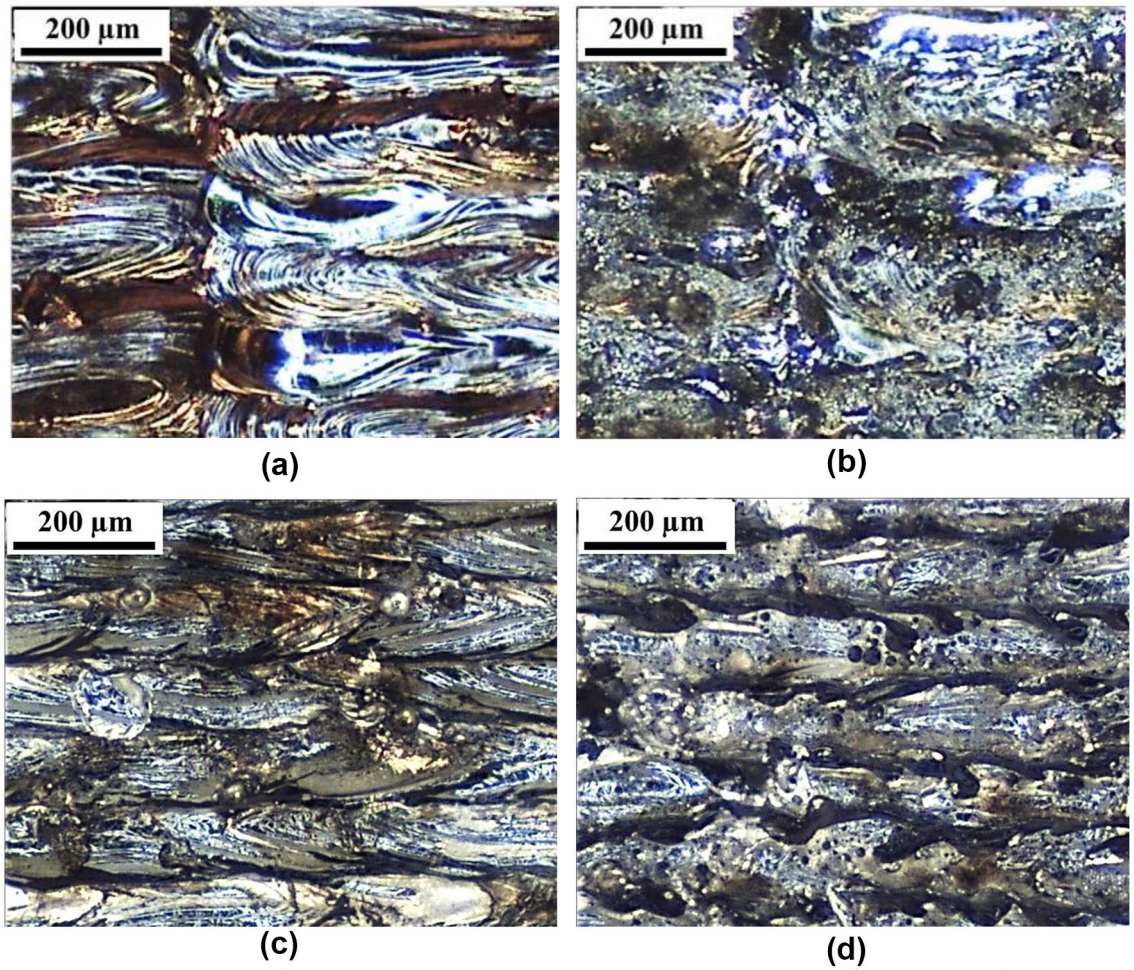

Fig. 3 Microscope images showing the surface of Al_2O_3 nanoparticle modified vs. unmodified standard materials after LBM **a** standard material Hastelloy X (2.4665), **b** nanoparticle modified standard material Hastelloy X (2.4665), **c** standard material tool steel (1.2709), **d** nanoparticle modified standard material tool steel (1.2709)

nanoparticle modified materials are significantly better in its bulk than anticipated from the surface quality, as discussed in the following.

3.2 Structure analysis of nanoparticle modified materials

Figure 4 depicts optical microscope images showing microsections of the Al_2O_3 nanoparticle modified materials (Fig. 4b, d) in comparison to unmodified standard materials (Fig. 4a, c). The nanoparticles clearly affect the microstructure of the composite materials compared to the standard materials.

It could be estimated that the dark areas in the images occur from voids that are a result of the imperfect welding process if Al_2O_3 nanoparticles are present on educt powders surface. But these void-like structures are no voids. Further investigations confirmed that these structures are dense particulates rather than gaseous voids. Nevertheless, the melting behavior of the modified standard materials appears to be worse compared to the unmodified standard materials. It seems that a very dense material structure is achieved. For nanoparticle modified powders the number, size and shape of the very small and round gaseous voids are similar to those of the non-modified powders. The particulates visible in the electron microscope images are bigger than typical voids and their geometry is different. In most cases their geometry is sharp edged. These results show that the nanoparticles tend to merge in the material structure, fabricating micro particulates. This in turn indicates that also the nanoparticle material Al_2O_3 has been sintered or partly molten during laser irradiation. During re-solidification the nanoparticles might merge together. Furthermore, the particulates are homogeneously distributed across the sample. Interestingly the particulates of the two modified standard materials are different in their chemical composition (see Fig. 5). Particulates formed after LBM in the modified standard material Hastelloy X

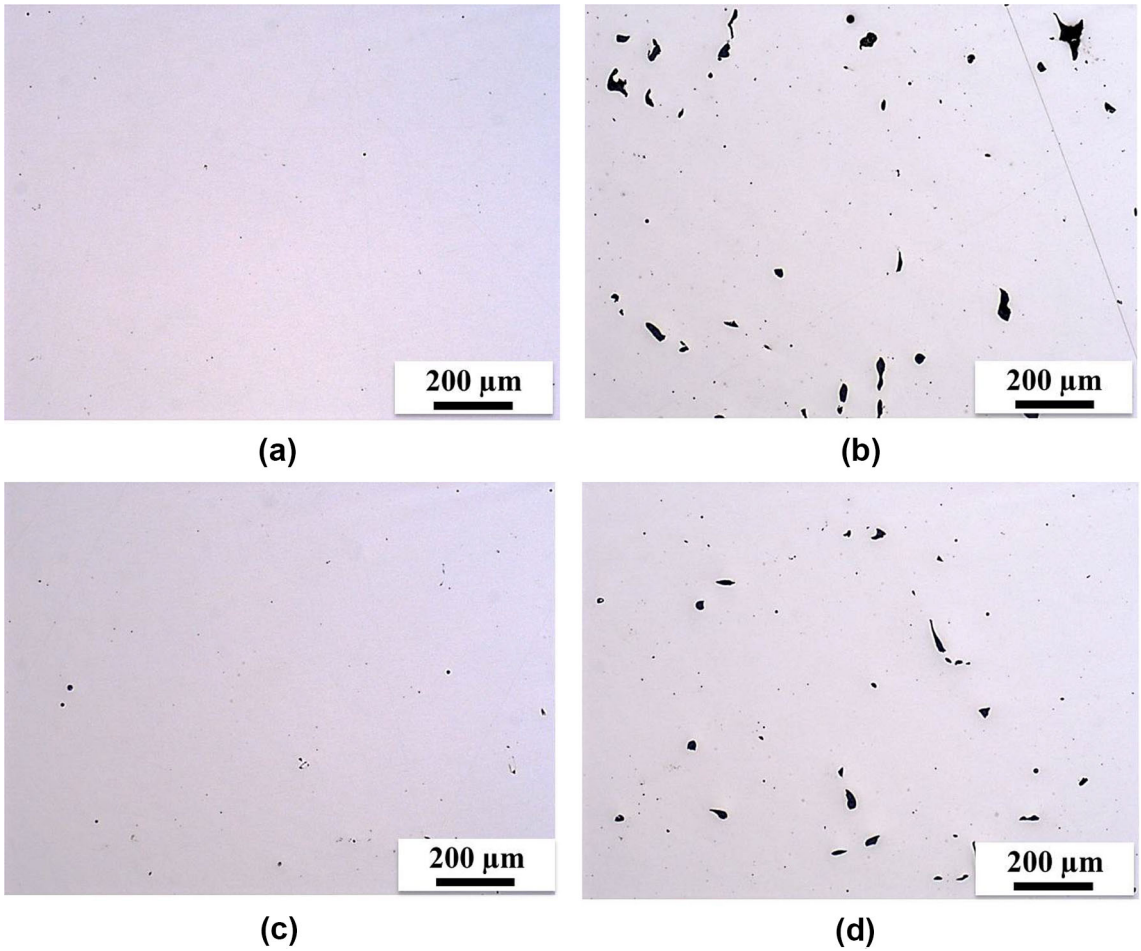

Fig. 4 Electron microscope images showing transverse microsections of Al_2O_3 nanoparticle modified vs. unmodified standard materials **a** standard material Hastelloy X (2.4665), **b** nanoparticle modified standard material Hastelloy X (2.4665), **c** standard material tool steel (1.2709), **d** nanoparticle modified standard material tool steel (1.2709)

(2.4665) show mainly Al-content and O-content. This could be expected if only the Al_2O_3 nanoparticles fuse in groups. Only residual amounts of the elements from the host material can be detected. An unexpected chemical composition of the particulates can be found in the nanoparticle modified material tool steel (1.2709). A significant increase of Ti-content up to 13 wt% is observed (cf. Fig. 10 in Sect. 5). The Ti-content inside of the particulates results from the surrounding standard tool steel (1.2709). The amount of the Ti-content in the tool steel is 0.69 wt% (cf. Fig. 10 in Sect. 5) what is approximately 5 times higher compared to the amount of Ti in Hastelloy X with <0.07% (cf. Fig. 11 in Sect. 5). The EDX analysis of the modified standard material Hastelloy X (2.4665) also reveals a slight enrichment of the Ti-content inside the Al_2O_3 precipitates, consistent with the small amount of Ti in the host material. Presumably Ti diffuses into the Al_2O_3 and forms a high temperature $Al_2TiO_5 + Al_2O_3$ solid solution [28]. More complicated ternary solid solutions of the form of Fe2-2xAl2xTiO5 are also possible and would extend the phase stability to lower temperatures, but appear rather unlikely because of the low Fe content (4.40 wt%) observed in the precipitates (cf. Fig. 10 in Sect. 5). The exact mechanism behind the Ti enrichment inside the precipitates is not clear at the moment and requires further investigation.

Figure 6 depicts a higher magnification of the microstructure taken from a particulate of the modified standard material tool steel (1.2709).

A fine network of bright lines up to the boundary of the particulate becomes visible at higher magnification which is observed more or less distinctive in all particulates. A careful EDX-analysis (not shown) identifies this bright lines as host material, enclosing Al_2O_3 grains which appear as dark areas in the SEM image. The well-defined boundaries between Al_2O_3 and host material nicely shows that the Al_2O_3 remains insoluble during the complete LBM process. Furthermore, the irregular shape of the particulates and the occurrence of host material networks inside of the particulates indicate that the Al_2O_3 nanoparticles might be partially molten during the complete process. Nevertheless,

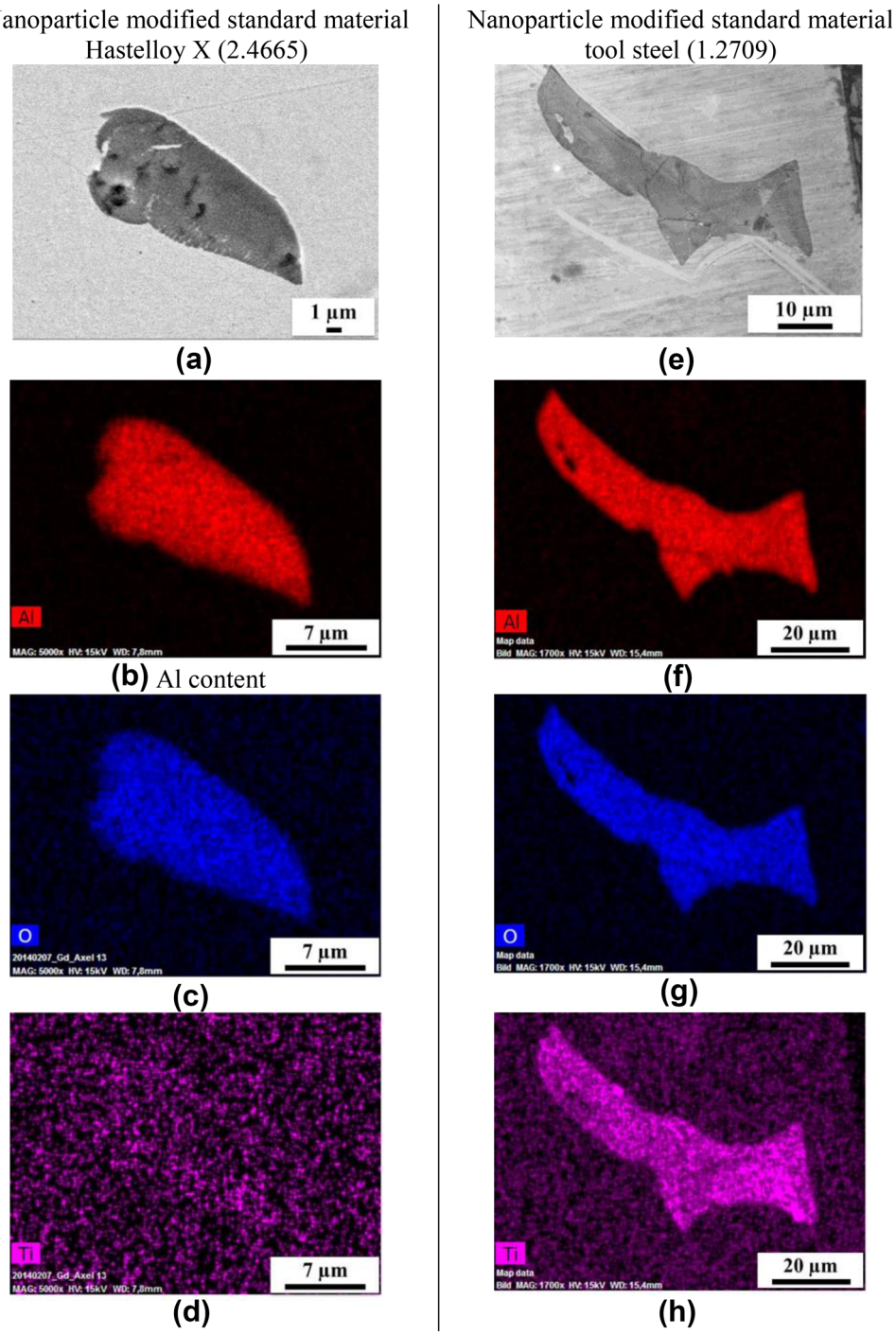

Fig. 5 Elemental analysis (EDX) of particulates of nanoparticle modified standard materials **a** P particulate recipitation Hastelloy X (2.4665), **b** Al content Hastelloy X (2.4665), **c** O content Hastelloy X (2.4665), **d** Ti-content Hastelloy X (2.4665), **e** particulate tool steel (1.2709), **f** Al content tool steel (1.2709), **g** O content tool steel (1.2709), **h** Ti-content tool steel (1.2709)

the LBM of Al_2O_3 nanoparticle enables at least fast sintering due to their small size and results in compact, fully densified particulates.

The Al_2O_3 nanoparticles attach to the host material and form different sized agglomerates with a random network of open pores (cf. Fig. 7c). During laser irradiation the host material melts rapidly and flows into the open pores of the Al_2O_3 agglomerates and at the same time sintering of the Al_2O_3 occurs and hence causes a densification of the initial agglomerates. Thus, the aim is to achieve a good wetting between the molten liquid phases of the host material on the one hand and the solid phase powder and solid nanoparticles on the other hand. During the development of the melt pool the agglomerates become mobile and may attach to each other depending on their initial distances, forming the different sized, irregular shaped particulates which can be observed.

Figure 8a shows a SEM image taken from the etched x–z cross section of the LBM processed modified material

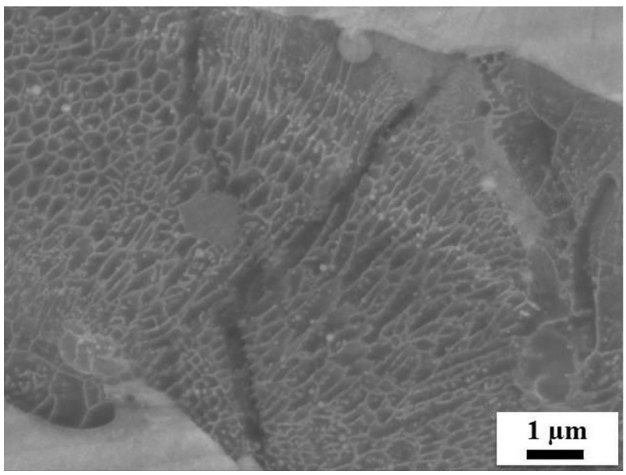

Fig. 6 Magnification of the particulate of the modified material tool steel (1.2709)

tool steel (1.2709). Single melt traces are visible bounded by thin lines on the specimen's surface. The lines are oriented in different directions due to the rotated exposure strategy during the LBM process. In the middle of the image a rectangular hardness indentation can be seen. Particulates are apparent as dark void-like structures. It turns out that particulates appear exclusively at the borders of melt traces, which underlines the theory of agglomeration of nanoparticles as a consequence of strong convection currents inside of the melt pool (see Fig. 7c). Inside of the melt traces even finer columnar structures can be identified as the characteristic microstructure of LBM produced materials (cf. Fig. 8b). Due to the rapid solidification process, LBM specimens often feature a columnar dendritic microstructure [5]. As a result of sequential melting and solidification in a layer by layer manner an epitaxial growth of dendrites is achieved, which follows the heat flux in the buildup direction. Therefore, the columnar dendritic crystals are mostly spread over several melt traces. Since the laser beam moves quickly and multidirectional over the powder bed surface, the preferred direction of the solidification front changes depending on the direction of process heat conduction. As a consequence different regions of uniform crystal orientations can be identified (regions 1, 2, 4 and 5 in Fig. 8b). Close to the particulate in the middle of Fig. 8b some regions occur where the uniform crystal orientation is distorted (regions 3 and 6 in Fig. 8b). Since these regions are located above (region 3) and below (region 6) the particulate, they form a line parallel to the build-up direction. It seems that during consolidation the agglomeration of Al_2O_3 particles affects the evolution of the heat flux in build-up direction and, therefore, the

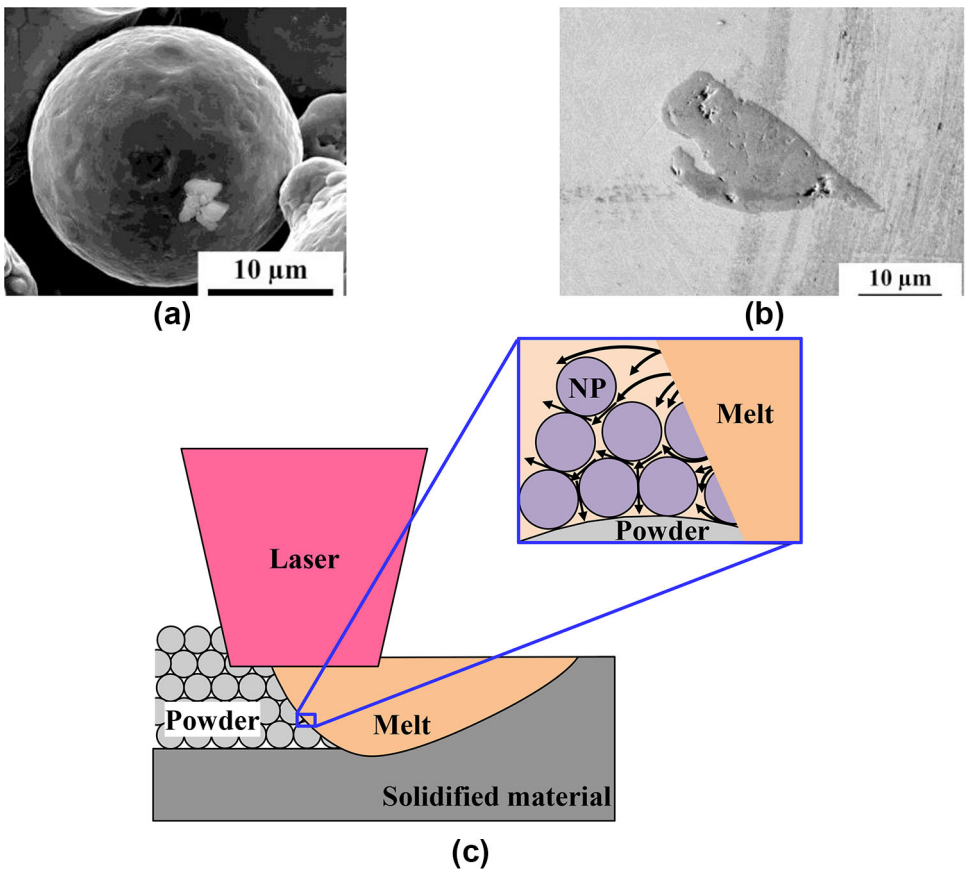

Fig. 7 Melt behavior of sintered or partly molten Al_2O_3 nanoparticles **a** typical size of reagent material, **b** typical size of particulates, **c** melt flow into open pores of Al_2O_3 agglomerates

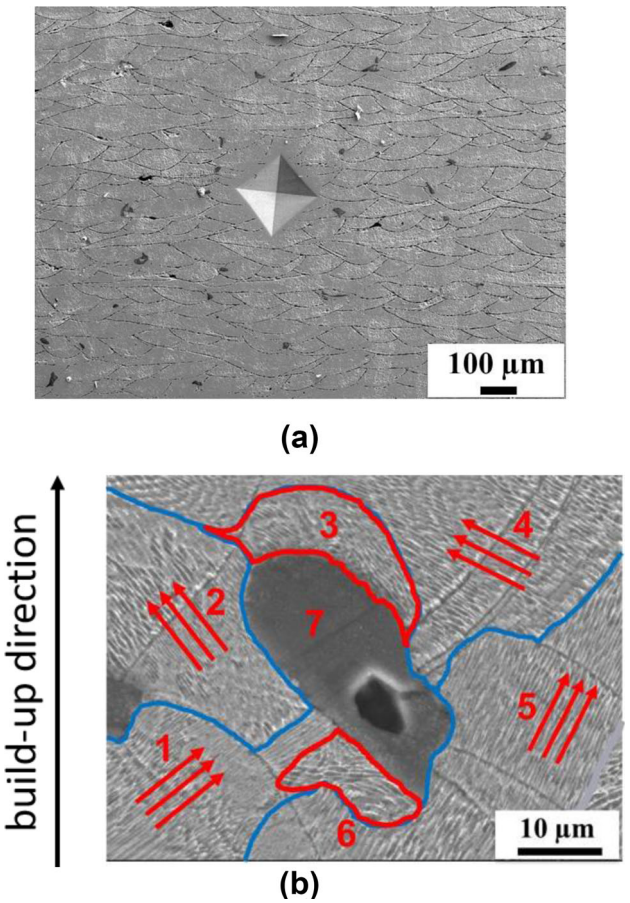

Fig. 8 SEM image of the etched longitudinal cross section of the LBM processed modified tool steel (1.2709) **a** overview of the specimens longitudinal cross section, **b** closer view at one single particulate (longitudinal cross section)

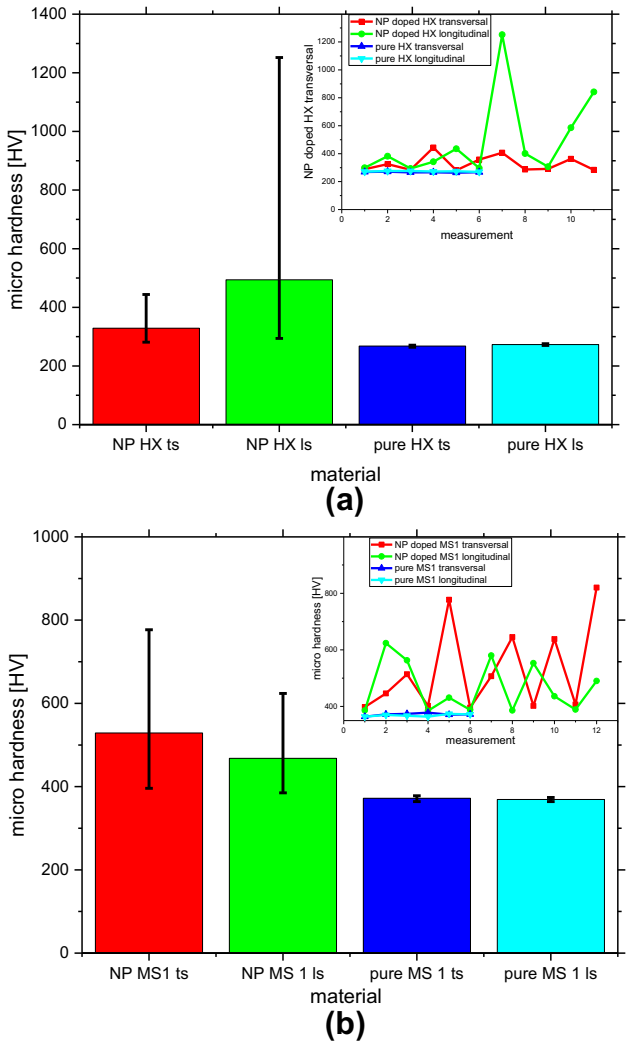

Fig. 9 Micro hardness measurements HV 0.2 according to DIN EN ISO 6507-1 **a** mean values (*bar chart*) and individual measured values (*inset*) of micro hardness of Hastelloy X (2.4665); Standard deviation of NP doped HX: transversal 56.9 HV and longitudinal 300.6 HV **b** Mean values (*bar chart*) and individual measured values (*inset*) of micro hardness of tool steel (1.2709); Standard deviation of NP doped MS1: transversal 154.1 HV and longitudinal 89.9 HV

evolution of the solidification front. Furthermore, the presence of the, maybe not fully molten, particulate may initiate the nucleation of crystals at the melt interface. Both in combination might influence the homogeneity of the resulting crystal orientation in region 3 and region 6. Since inside of region 2 and region 5 no particulate inhibits the nucleation and heat flow evolution in respect to the build-up direction, the resulting crystal orientation in these regions is not distorted.

3.3 Micro hardness of nanoparticle modified materials

In Fig. 9 both, the mean values and the individual measured values of micro hardness of nanoparticle modified materials are shown and compared to the standard materials. Both nanoparticle modified standard materials show a significant increase in hardness across the entire structure compared to the host materials. The mean value of nanoparticle modified Hastelloy X material in the transverse section is 328.5 HV. Compared to the standard Hastelloy X material in the same direction (∅ 267.5 HV) this is about 22.8% higher. Even more obvious is the comparison of the longitudinal section. Here the mean value of the nanoparticle modified Hastelloy X material in the longitudinal section (494.3 HV) is 80.8% higher compared to the host material in the same direction (∅ 273.3 HV). Similar results can be observed looking at the tool steel material where the mean value of nanoparticle modified tool steel material in the transverse section is 529.3 HV. In average this is 157.5 HV higher compared to the mean value of the regular tool steel material (371.8 HV). At the longitudinal section of the tool steel materials the two values differ from each other by 99.1 HV (=26.9%). Furthermore, all observed single values of the nanoparticle

modified materials are higher than the maximum values of the non-modified materials.

The values of the nanoparticle modified materials vary in a wide range, depending on the location of the indentation pyramid. The maximum value of micro hardness of nanoparticle modified Hastelloy X (2.4665) is 1252 HV and 820 HV at nanoparticle modified tool steel (1.2709). Both maximum values were measured directly on or next to the surface of one of the precipitates. It can be concluded that the micro hardness increases significantly in the vicinity of the precipitates. In addition, the precipitates are more or less uniformly distributed in the material structure. This in turn may lead to crystal defects and to hindrances of the movement of dislocations in the matrix which in turn could be responsible for higher hardness values. This strong variation cannot be observed at the standard materials. On the contrary the standard deviation of the tool steel material is 4.6 and 2.4 HV at the Hastelloy X material.

4 Conclusions

The integration of nanoparticles during laser beam melting of standard materials improves material characteristics. It can be seen that the implementation of nanoparticles strongly increases the mechanical properties of the material even though the nanoparticles were agglomerated to micro sized particulates. In detail the micro hardness of the microstructure has been investigated. Both nanoparticle modified materials show a significant increase in microhardness in the sphere of influence around the particulates. During the melting of the modified powder materials nanoparticles form agglomerates due to the strong convection currents and different phase compositions inside of the melt pool. These agglomerates finally result in particulates, which are mostly dense sintered or partly molten structures, infiltrated by small web-like structures from the molten host material. As a consequence of agglomeration and melt pool dynamics the particulates appear exclusively at the borders of single melt traces. When additional layers solidify on already created layers the heat flux is affected by the particulates position and thermal properties, which finally leads to local disturbances of the preferred grain orientations. Ongoing investigations are carried out to determine the influence of the nanoparticle material itself and the processing parameters on the structure and mechanical properties. Also the content of the nanoparticles being used for modifying the standard materials will be investigated in future work to optimize nanocomposite parts. In addition both base powders, tool steel (1.2709) and Hastelloy X (2.4665), are made of precipitation hardening materials which traditionally achieve their outstanding mechanical properties due to the precipitation of intermetallic phases. With regard to this, it is interesting how the presence of nanoparticles in the matrix is influencing the hardening behavior and hardening effect. This will also be investigated in future work.

Acknowledgements The authors thank Prof. Stephan Barcikowski and Dr. Marcus Lau for the nanoparticle modification of the standard materials. The authors also thank Prof. Alfons Fischer and his team for the utilization of analysis devices and support regarding light microscopy, sample preparation, etching and micro hardness measurements. Furthermore, the authors thank Sebastian Platt for his contribution within his student assistant contract.

Compliance with ethical standards

Conflict of interest On behalf of all authors, the corresponding author states that there is no conflict of interest.

Appendix

Figures 10 and 11.

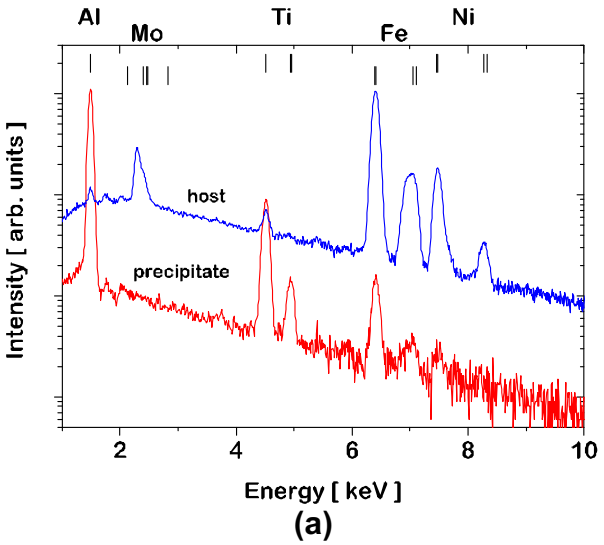

(a)

Element	Host	Precipitate
Fe	62.52±1.9 wt-%	4.4±0.2 wt-%
Ni	16.75±0.6 wt-%	0.7±0.1 wt-%
Co	8.61±0.3 wt-%	0.39±0.1 wt-%
Mo	4.20±0.2 wt-%	≤ 0.05 wt-%
Ti	0.69±0.1 wt-%	12.90±0.45 wt-%
Al	0.26±0.1 wt-%	33.08±1.7 wt-%
Cr	0.18±0.1 wt-%	≤ 0.09 wt-%
Cu	0.17±0.1 wt-%	≤ 0.01 wt-%
C	5.70±0.8 wt-%	4.41±1.1 wt-%
Mn	0.22±0.1 wt-%	0.12±0.04 wt-%
Si	≤ 0.06 wt-%	≤ 0.04 wt-%
P	≤ 0.01 wt-%	≤ 0.04 wt-%
S	0.28±0.1 wt-%	≤ 0.01 wt-%
O	0.39±0.1 wt-%	43.77±5.73 wt-%

(b)

Fig. 10 EDX analysis of nanoparticle modified tool steel (1.2709), **a** EDX spectra taken at a precipitate and host material, **b** elemental composition obtained from EDX spectra

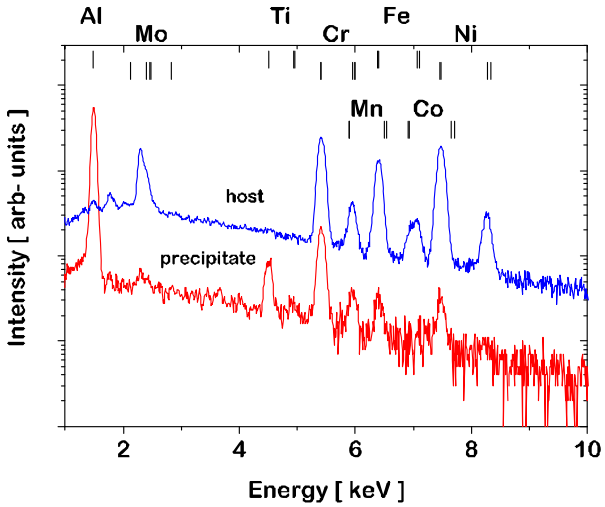

(a)

Element	Host	Precipitate
Ni	39.50±1.3 wt-%	2.14±0.2 wt-%
Cr	18.87±0.6 wt-%	7.48±0.3 wt-%
Fe	15.85±0.5 wt-%	1.30±0.1 wt-%
Mo	7.52±0.3 wt-%	0.64±0.1 wt-%
O	1.02±0.2 wt-%	41.19±5.1 wt-%
Co	1.46±0.1 wt-%	≤ 0.01 wt-%
C	15.07±2.1 wt-%	9.90±2 wt-%
Si	≤ 0.04 wt-%	≤ 0.01 wt-%
Mn	≤ 0.01 wt-%	≤ 0.01 wt-%
S	≤ 0.13 wt-%	≤ 0.01 wt-%
P	≤ 0.01 wt-%	≤ 0.01 wt-%
Se	≤ 0.01 wt-%	≤ 0.01 wt-%
Cu	≤ 0.26 wt-%	≤ 0.01 wt-%
Al	≤ 0.19 wt-%	35.49±1.6 wt-%
Ti	≤ 0.07 wt-%	1.85±0.1 wt-%
W	≤ 0.01 wt-%	≤ 0.01 wt-%

(b)

Fig. 11 EDX analysis of nanoparticle modified Hastelloy X (2.4665), **a** EDX spectra taken at a precipitate and host material, **b** elemental composition obtained from EDX spectra

References

1. VDI-Guideline 3405 (2014) Additive manufacturing processes, rapid manufacturing—basics, definitions, processes
2. ISO/ASTM 52900 (2015) Additive manufacturing, general principles, terminology
3. Meiners W (1999) Direktes Selektives Laser-Sintern einkomponentiger metallischer Werkstoffe. Dissertation, RWTH Aachen University
4. Wagner C (2002) Untersuchungen zum Selektiven Lasersintern von Metallen, Dissertation, RWTH Aachen University
5. Sehrt JT (2010) Möglichkeiten und Grenzen bei der generativen Herstellung metallischer Bauteile durch das Strahlschmelzverfahren. Dissertation, University of Duisburg-Essen
6. Harrision NJ, Todd I, Mumtaz K (2015) Reduction of micro-cracking in nickel superalloys processed by selective laser melting: a fundamental alloy design approach. Acta Mater 94:59–68
7. Schmidkte K, Palm F, Hawkins A, Emmelmann C (2011) Process and mechanical properties: applicability of a scandium modified Al-alloy for laser additive manufacturing. Phys Procedia 12:336–379
8. Gu D, Shen Y (2007) Effects of dispersion technique and component ratio on densification and microstructure of multi-component Cu-based metal powder in direct laser sintering. J Mater Process Technol 182:564–573
9. Gu D, Meiners W (2010) Microstructure characteristics and formation mechanism of in situ WC cemented carbide based hardmetals prepared by selective laser melting. Mater Sci Eng, A 527:7585–7592
10. Yugang D, Yuan Z, Yiping T, Dichen L (2011) Nano-TiO_2-modified photosensitive resin for RP. Rapid Prototyp J 17(4):247–252
11. Chiu S-H, Wicaksono ST, Chen K-T, Chen C-Y (2015) Mechanical and thermal properties of photopolymer/CB (carbon black) nanocomposite for rapid prototyping. Rapid Prototyp J 21(3):262–269
12. Gu D, Hagedorn Y-C, Meiners W, Wissenbach K, Poprawe R (2014) Nanocrystalline TiC reinforced Ti matrix bulk-form nanocomposites by selective laser melting (SLM): densification, growth mechanism and wear behavior. Compos Sci Technol 71:1612–1620
13. Gu D, Wang H, Zhang G (2014) Selective laser melting additive manufacturing of Ti-based nanocomposites: the role of nanopowder. Metall Mater Trans A 45A:464–476
14. Gu D, Meng G, Li C, Meiners W, Poprawe R (2012) Selective laser melting of TiC/Ti bulk nanocomposites: influence of nanoscale reinforcement. Scr Mater 67:185–188
15. Gu D, Wang H, Chang F, Dai D, Yuan P, Hagedorn Y-C, Meiners W (2014) Selective laser melting additive manufacturing of TiC/AlSi10 Mg bulk-form nanocomposites with tailored microstructures and properties. Phys Procedia 56:108–116
16. Gu D, Wang H, Dai D, Yuan P, Meiners W, Poprawe R (2015) Rapid fabrication of Al-based bulk-form nanocomposites with novel reinforcement and enhanced performance by selective laser melting. Scr Mater 96:25–28
17. Gu D, Wang Z, Shen Y, Li Q, Li Y (2009) In-situ TiC particle reinforced Ti-Al matrix composites: powder preparation by mechanical alloying and selective laser melting behavior. Appl Surf Sci 255:9230–9240
18. Chang F, Gu D, Dai D, Yuan P (2015) Selective laser melting of in situ Al4SiC4 + SiC hybrid reinforced Al matrix composites: influence of starting SiC particle size. Surf Coat Technol 272:15–24
19. Lau M, Niemann R, Bartsch M, O'Neill W, Barcikowski S (2014) Near-field-enhanced, off-resonant laser sintering of semiconductor particles for additive manufacturing of dispersed Au–ZnO-micro/nano hybrid structures. Appl Phys A 114:1023–10301
20. Crespo-Monteiro N, Destouches N, Saviot L, Reynuad S, Epicier T, Gamet E, Bios L, Boukenter A (2012) One-step microstructuring of TiO_2 and Ag-TiO_2 films by continuous wave laser processing in the UV and visible ranges. J Phys Chem C 116:26857–26864
21. Schade L, Franzka S, Dzialkowski K, Hardt S, Wiggers H, Reichenberger S, Wagener P, Hartmann N (2015) Resonant photothermal laser processing of hybrid gold/titania nanoparticle films. Appl Surf Sci 336:48–52
22. Lau M, Barcikowski S (2015) Quantification of mass-specific laser energy input converted into particle properties during picosecond pulsed laser fragmentation of zinc oxide and boron carbide in liquids. Appl Surf Sci 348:22–29
23. King WE, Anderson AT, Ferencz RM, Hodge NE, Kamath C, Khairallah SA, Rubenchik AM (2015) Laser powder bed fusion additive manufacturing of metals; physics, computational and materials challenges. Appl Phys Rev 2:041304. doi:10.1063/1.4937809

24. Körner C, Bauereiß A, Attar E (2013) Fundamental consolidation mechanisms during selective beam melting of powders. Model Simul Mater Sci Eng. doi:10.1088/0965-0390/21/8/085011
25. Kruth J-P, Levy G, Klocke F, Childs THC (2007) Consolidation phenomena in laser and powder-bed based layered manufacturing. Ann CIRP. doi:10.1016/j.cirp.2007.10.004
26. Sehrt JT, Witt G (2011) Manufacturing of defined porous metal structures using the beam melting technology, In: Bártolo PJ (Hrsg.): Proceedings of the 5th international conference on advanced research in virtual and rapid prototyping, Leiria, Portugal, pp 639–644
27. Kleszczynski S, Sehrt JT, Witt G, zur Jacobsmühlen J (2012) Error detection in laser beam melting systems by high resolution imaging, international solid freeform fabrication symposium, The University of Texas at Austin, 9 th–11th August 2012
28. Pownceby MI, Constanti-Carey KK, Fisher-White MJ (2003) Subsolidus phase relationships in the system Fe_2O_3–Al_2O_3–TiO_2 between 1000 and 1300 °C. J Am Ceram Soc 86:975–980